

Semantic segmentation-based intelligent threshold-free feeder detection method for single-phase ground fault in distribution networks

Cui Hong, Heng-Yi Qiu, Jian-Hong Gao, Shuyue Lin and Mou-Fa Guo, *Member, IEEE*

Abstract—Feeder detection for single-phase ground fault (SPGF) is challenging in a resonant grounded system due to the difference in feeder capacitance to ground and the influence of the arc suppression coil. This paper utilizes semantic segmentation algorithms to implement feeder detection for SPGF in distribution networks. The proposed method overlays transient zero-sequence voltage (ZSV) derivatives and transient zero-sequence current (ZSC) waveforms on the same image. Then, a semantic segmentation algorithm is used to classify the pixel points of the image. The segmentation map output by the semantic segmentation algorithm contains category prediction results for each pixel in the input image. Detecting faulty feeder based on the number of pixels of different categories in the segmentation map can make the final decision-making process more transparent and easy to understand. The validity and adaptability of the proposed method have been confirmed through tests using both simulation and field data. The proposed method achieves an accuracy of over 95% on simulated data, even in the presence of noise interference and asynchronous sampling, etc. Furthermore, the proposed method achieves an accuracy of over 99% when applied to full-scale test data.

Index Terms—distribution network, single-phase ground fault, feeder detection, artificial intelligence, semantic segmentation

I. INTRODUCTION

THE SPGF is the predominant fault type, representing over 80% of the total fault occurrences[1]. In China, non-effective grounded systems are widely employed in medium voltage distribution networks[2]. A non-effectively grounded system, based on the different methods of neutral grounding, can be classified into an ungrounded and resonant grounded system[3]. Feeder detection of SPGF is challenging in a resonant grounded system due to the difference in feeder capacitance to ground and the influence of the arc suppression coil. If faults are not addressed promptly, they can pose significant safety risks, including but not limited to fire, equipment damage, and personal injury. Providing an accurate

and reliable method of detecting faulty feeder is essential to safeguard the secure and stable functioning of power systems and prevent the spread of accidents.

The existing faulty feeder detection methods mainly include threshold method and artificial intelligence method.

The threshold-based method employs threshold values of fault characteristics to identify faulty feeder. Wang et al. [4] conducted fault location by comparing the transient energy of fault section and non-fault section within the selected frequency band. Wei et al. [5] utilized transient energy and cosine similarity as features to achieve feeder detection using Laplace distribution and cumulative density function. Peng et al. [6] achieved feeder detection by comparing the transient zero-mode amplitude ratio at both ends of the feeder with the standard amplitude ratio. The choice of fault characteristics heavily relies on experience and is typically based on extensive experimentation and accumulated domain knowledge.

With the rise of machine learning, the application of artificial intelligence techniques in fault identification is becoming more widespread. Classification models dominate the field of artificial intelligence techniques applied to fault identification. Okumus and Nuroglu [7] applied wavelet transform to three-phase voltage and current data and utilized random forests for fault section identification after feature extraction. This paper employs artificial intelligence algorithms for fault classification without relying on fixed thresholds but still follows a signal-processing approach for fault feature extraction. The accuracy of feeder detection still relies on the effectiveness of the feature selection.

End-to-end deep learning, based on simple input data without relying on other complex operations, has shown remarkable performance in feature extraction and classification. Convolutional neural networks (CNN), known for their powerful feature extraction capabilities in image processing, have found extensive applications in various areas of vision research. Guo et al. [8] converted ZSC into grayscale image and then utilized CNN for feeder detection. Yuan and Jiao. [9] employed a specific order to superimpose different feeder ZSC in different images and utilized a CNN embedded with an attention learning block for feeder detection. Yuan et al. [10] superimposed ZSV and ZSC on the same image and employed a CNN with spatial attention residual learning blocks for feeder detection. Yuan and Jiao. [11] used CNN and long short-term memory networks to extract features from ZSC data for feeder detection. Gao et al. [12] accomplished

This work is supported in part by the National Natural Science Foundation of China under Award 51677030, in part by the Natural Science Foundation of Fujian Province, China under Award 2023J01230134. (Corresponding author: Mou-Fa Guo.)

Cui Hong, Heng-Yi Qiu, Jian-Hong Gao and Mou-Fa Guo are with College of Electrical Engineering and Automation, Fuzhou University, Fuzhou 350108, China (e-mail: hongcui@fzu.edu.cn, 1438050250@qq.com, gaojianhong1994@foxmail.com, gmf@fzu.edu.cn).

S. Lin is with the School of Engineering, University of Hull, Hull HU6 7RX, U.K. (e-mail: S.Lin@hull.ac.uk).

feeder detection by fusing the ZSC waveform of the first half-cycle and employing a one-dimensional CNN. Yuan and Jiao [13] superimposed the ZSC waveforms of all feeders on the same image and then used a fully convolutional network (FCN) and fault trust degree to detect faulty feeder. The literature [8-12] applied deep learning algorithms for feeder detection, which can automatically extract features and perform classification by constructing deep neural networks and leveraging large amounts of data without relying on manually-designed feature extraction. However, the final decision process for feeder detection is difficult to understand.

To address the above issues, this paper presents a threshold-free method for detecting faulty feeder by utilizing a semantic segmentation algorithm. Semantic segmentation is the classification of the input image at the pixel level and finally outputs a segmentation map. It has been widely applied in remote sensing images[14] and biomedical images[15]. This paper utilizes the superimposed image of ZSV derivative and ZSC as the input for a semantic segmentation algorithm, which generates predicted labels for each pixel of the image. The feeder detection results rely on the segmentation map generated by the semantic segmentation algorithm, combined with additional criteria. The main contributions are summarized as follows.

1) Faulty feeder can be detected even if start-up moment inaccuracy. This paper uses a semantic segmentation algorithm with pixel-level classification to detect faulty feeder. In cases where the deviation between the moment of start-up and the actual moment of failure causes the pixels occupied by part of the waveform in the image to be misclassified, it is still possible to accurately detect faulty feeder in conjunction with the feeder detection criterion used in this paper.

2) The final decision-making process is more transparent and understandable. Each value in the segmentation map corresponds to the classification prediction result for each pixel in the input image. When the number of pixels occupied by a faulty waveform is greater than those occupied by a non-faulty waveform in the segmentation map, the corresponding feeder is judged to be a faulty feeder. Otherwise, it is a sound feeder, making the final decision for feeder detection more transparent and understandable.

The subsequent sections of this paper are structured as follows. Section 2 analyses the relationship between ZSV and ZSC when a SPGF occurs in the distribution network. Section 3 describes the implementation process of the proposed method. Section 4 presents experimental validation, which includes testing of simulation and field data, as well as testing of the adaptability of the proposed method. Finally, Section 5 summarizes the study.

II. ANALYSIS OF THE PRINCIPLE OF SINGLE-PHASE GROUND FAULT IN DISTRIBUTION NETWORK

When a SPGF occurs, the transient zero-sequence equivalent network can be simplified as depicted in Fig. 1, where Z for three times the sum of the transition impedance, line resistance and line inductance, L for three times the

inductance of the arc suppression coil, u_f for the SPGF current through the zero-sequence impedance generated voltage, C_0 for the zero-sequence capacitance to ground.

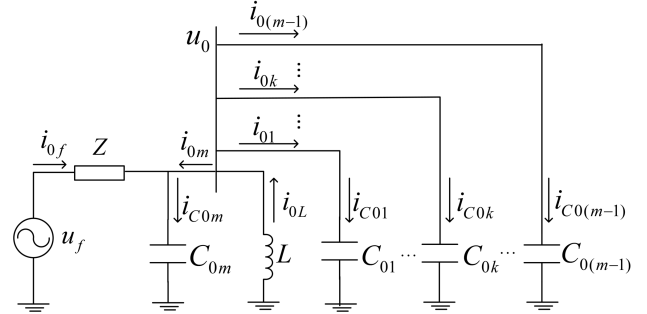


Fig. 1. Equivalent network of single-phase ground fault.

For resonant grounded system:

$$i_{0k} = i_{C0k} = C_{0k} \frac{du_0}{dt} \quad (1)$$

$$i_{0m} = -(i_{0\Sigma} - i_{C0m} - i_{0L}) = i_{0L} - (C_{0\Sigma} - C_{0m}) \frac{du_0}{dt} \quad (2)$$

Where i_{0k} is the sound feeder ZSC, i_{0m} is the faulty feeder ZSC, du_0/dt is the ZSV derivative.

A typical waveform when a SPGF occurs is shown in Fig. 2. Fig. 2 displays the waveforms of ZSV derivative and ZSC of four feeders, consisting of three sound feeders and one faulty feeder.

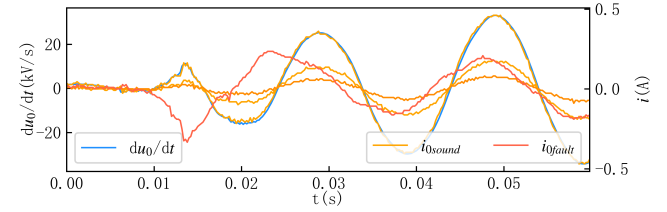


Fig. 2. Typical waveform of single-phase ground fault.

Due to the impact of the arc suppression coil, the polarity of the ZSV derivative and ZSC for a faulty feeder changes from opposite to the same. The polarity of the ZSV derivative and ZSC for sound feeders is the same. Fault characteristics such as steady-state current polarity and amplitude no longer meet the requirements of feeder detection. Therefore, the non-effective grounded system can use the transient ZSV derivative and ZSC relationship for feeder detection.

III. FEEDER DETECTION METHOD

A. Framework for feeder detection method

This paper presents a feeder detection method utilizing a fully convolutional network, and its framework is depicted in Fig. 3. The developed prototype is a SPGF feeder detection module, placed on a 10kV distribution feeder pole. The data acquisition module collects ZSV and ZSC data and then transfers it to the Raspberry Pi 4B for data processing and feeder detection. The fault is detected and the moment of occurrence is determined using our team's start-up algorithm[16]. In data preprocessing, the ZSV and ZSC are first denoised and filtered. Next, the derivative operation is performed on the ZSV, and the transient waveform of one cycle after the fault point is extracted and normalized. Subsequently, the normalized waveforms are superimposed on

the same image as input for the FCN during training. The trained FCN can classify each pixel in the input image, ultimately generating a segmentation map. Each value in the segmentation map corresponds to the classification prediction result for each pixel point in the input image. The category of the corresponding pixel for the background, faulty feeder waveform, and sound feeder waveform are denoted by 0, 1, and 2, respectively. For

visualization purposes, label 0 is displayed in grey, 1 in red, and 2 in blue. If the number of pixels labeled as 1 in the segmentation map is greater than those labeled as 2, the corresponding feeder is judged to be the faulty feeder. Otherwise, it is identified to be the sound feeder. Finally, the result judged by the feeder detection algorithm is sent to the dispatch center.

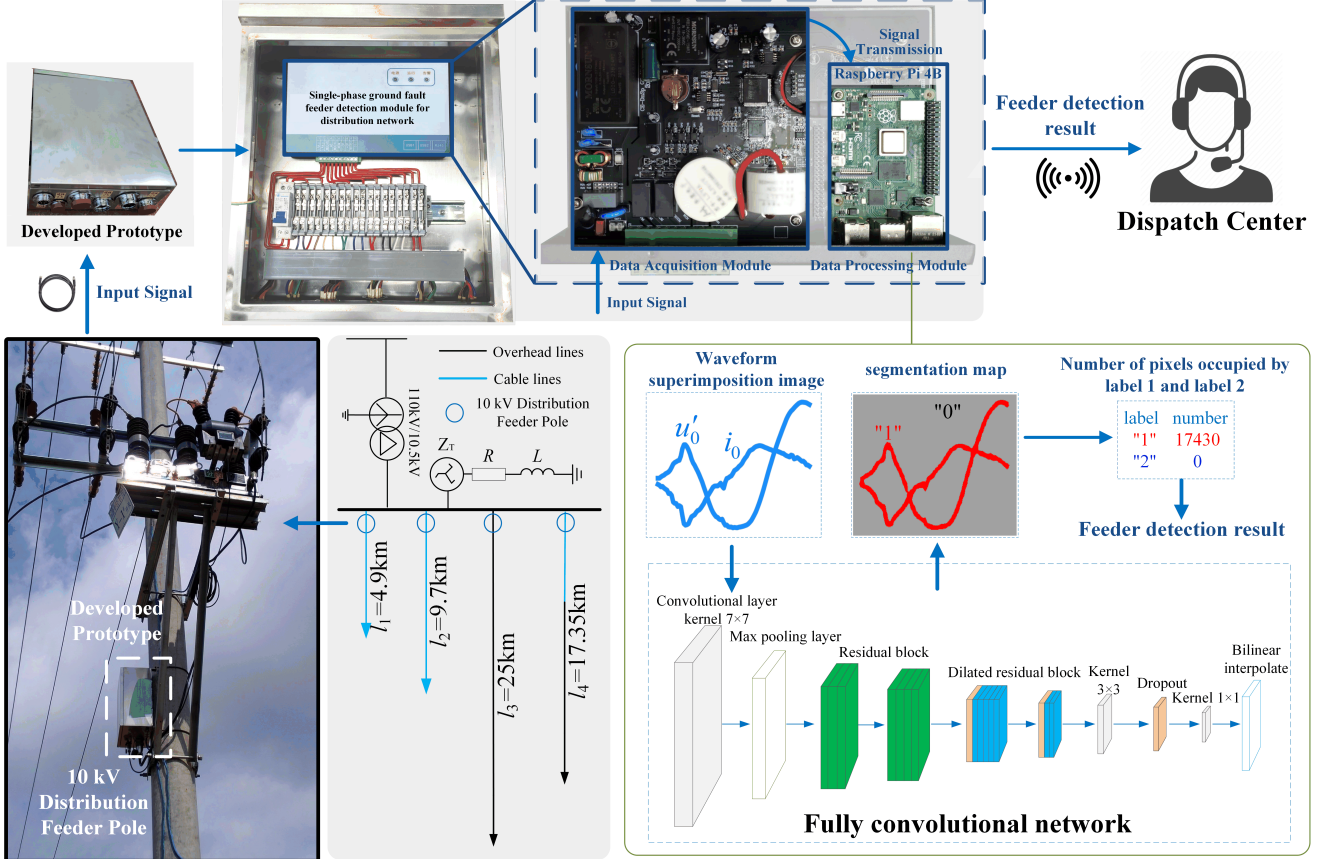


Fig. 3. Framework for feeder detection method.

B. Waveform processing and image creation

For the collected ZSV and ZSC data, the ZSV and ZSC are first denoised and filtered, then the derivative operation is performed on the ZSV, and the transient waveform of one cycle after the fault point is extracted and normalized.

The amplitude of ZSV is directly normalized to $[-1, 1]$, as shown in Equation (3). The ZSC is processed using Equation (4).

$$u_0^{\text{nor}}(t) = \frac{u_0(t)}{\max(|u_0(t)|)} \quad (3)$$

$$i_0^{\text{nor}}(t) = \frac{0.6 \times i_0(t)}{\max(|i_0(t)|)} \quad (4)$$

Where u_0^{nor} is the normalized ZSV.

Subsequently, the normalized transient ZSV and transient ZSC waveforms are superimposed on the same image. Pixel-level labeling of the superimposed waveform image is also required before model training, as shown in Fig. 4. The categories corresponding to pixels in the background, faulty feeder waveform, and sound feeder waveform are labeled as 0, 1, and 2, respectively. For visualization purposes, labels 0, 1,

and 2 are displayed in grey, red, and blue, respectively.

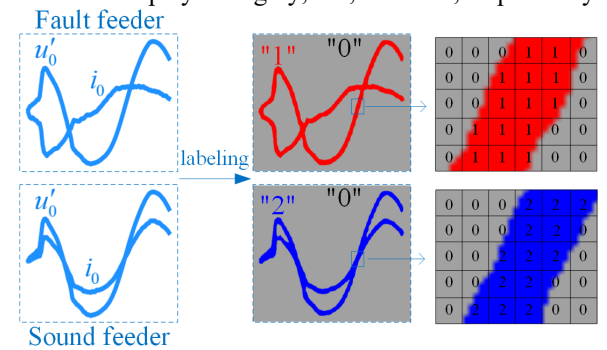


Fig. 4. Pixel-level labeling of waveform superimposed image.

C. Fully Convolutional Network

The structure of the FCN is depicted in Fig. 5. A FCN is constructed based on the ResNet-50 architecture, where the fully connected layers are replaced with convolutional layers, allowing for the processing of arbitrary-sized input images. Bilinear interpolation is used for up-sampling operations, resulting in a segmentation map with the same size as the input image, enabling semantic segmentation of the image.

Dilated convolution is used in FCN to increase the perception field without changing the convolution kernel's size[17]. Dilated convolution causes a grid effect during the convolution process. An appropriate dilation rate must be chosen to achieve adequate coverage of the input image to prevent loss of image information. The original ResNet50 performs down-sampling on the input image by a factor of 32. The utilization of dilated convolutions in ResNet50 leads to a decrease of the down-sampling factor to 8, consequently resulting in a better effect during up-sampling.

In FCN, the purpose of 1x1 convolution is to adjust the number of channels in the output of convolutional layers to

accommodate subsequent up-sampling tasks better. Bilinear interpolation is used to up-sample the adjusted feature maps to the same size as the input image to generate pixel-level semantic segmentation results.

The loss function used in this paper is the cross entropy loss function, which is applied to gauge the disparity between the model's predicted outcome and the true label. The formula is shown in (5).

$$H(p, q) = -\sum_i p_i \log(q_i) \quad (5)$$

Where p_i is the true label value, q_i is the predicted value.

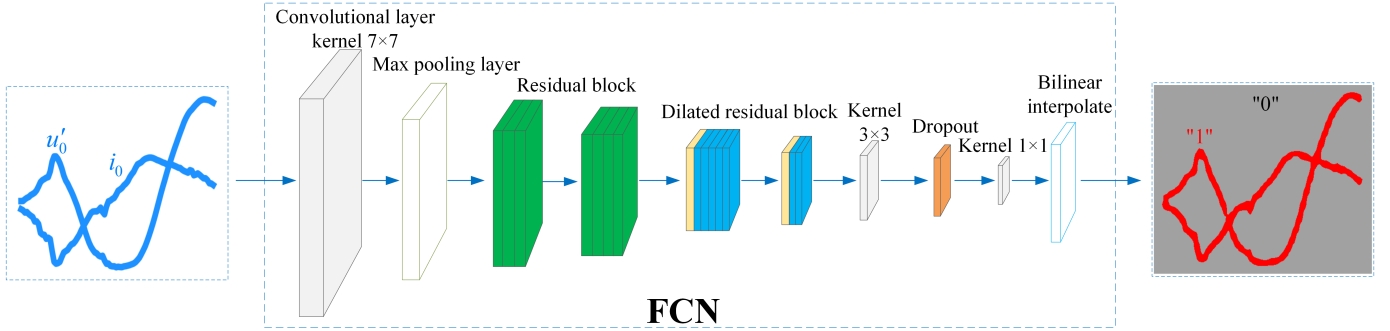


Fig. 5. Architecture of fully convolutional network.

D. Feeder detection criteria

The output of FCN is a segmentation map, where each value corresponds to the predicted classification result for each pixel in the input image. Where label 0, label 1, and label 2 are the pixel categories corresponding to the background, faulty feeder waveform, and sound feeder waveform, respectively. If the number of pixels labeled as 1 in the segmentation map is greater than those labeled as 2, the corresponding feeder is judged to be the faulty feeder. Otherwise, it is judged to be the sound feeder.

IV. EXPERIMENTAL VERIFICATION

A. Software simulation models

A simulation model for a 10kV distribution network was built using PSCAD/EMTDC, as depicted in Fig. 6. The lines consist of a combination of overhead lines and cable lines, totaling six lines. The Bergeron model was used for the lines, and the corresponding parameters are provided in Table I. The system operates in overcompensation mode with an overcompensation level of 5%, and the sampling frequency is 5 kHz. Simulation data are obtained for different fault locations, fault resistances, fault phase angles, and SPGF models in the case of a three-phase unbalance. Table II lists the distribution of the above failure scenarios.

TABLE I

LINE PARAMETERS IN THE DISTRIBUTION NETWORK SIMULATION MODEL

Line type	Sequential component	Resistance Ω/km	Inductance mH/km	Capacitance $\mu\text{F}/\text{km}$
Cable lines	Positive	0.27	0.255	0.339
	Zero	2.7	1.019	0.28
Overhead lines	Positive	0.17	1.21	0.0097
	Zero	0.23	5.478	0.008

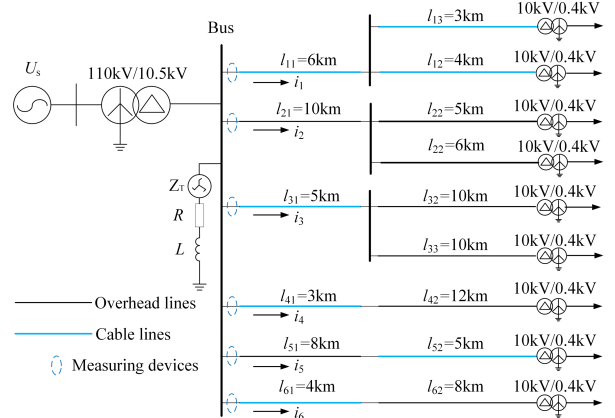


Fig. 6. Distribution network simulation model

TABLE II

FAILURE SCENARIOS INCLUDED IN THE TRAINING SET	
PSCAD simulation	Training samples
Fault location	All lines
Fault resistance	$5\Omega/10\Omega/50\Omega/100\Omega/300\Omega/500\Omega/1\text{k}\Omega/2\text{k}\Omega/3\text{k}\Omega/5\text{k}\Omega$
Fault phase angle	$0^\circ / 30^\circ / 60^\circ / 90^\circ / 120^\circ / 150^\circ$
Single-phase ground fault model	Resistance/Mayr model/Cassie model/Cybernetic model/Emanuel model

The superimposed image of the transient ZSV derivative and the transient ZSC waveform of each feeder is used as a training sample, and pixel-level labeling is performed on them. A total of 2520 samples are selected as the training set, with a 1:1 ratio between fault samples and non-fault samples. The waveform superimposed images are input to the FCN to train the model, and the best model is saved after training is completed. The computer parameters used to train the FCN are shown in Table III. The FCN training uses the Pytorch framework with 100 epochs and a learning rate of 0.0001.

TABLE III
COMPUTER PARAMETERS FOR TRAINING SEMANTIC
SEGMENTATION ALGORITHM

Computer configurations	Parameters
CPU	Intel(R) Core (TM) i9-12900K
Memory	64GB
Hard Disk	3.6T
Video Cards	NVIDIA GeForce GTX3070

To assess the performance of the model on the simulated data, simulation data from the training and testing sets were utilized for testing. The testing results are presented in Table IV. The indicators employed are presented in Equation (6), where Acc denotes accuracy, Pre denotes precision, and Rec denotes recall, $Sens$ denotes sensitivity, $Spec$ denotes specificity. The accuracy of the simulated data in both the training and testing sets is 100%, indicating excellent performance of the model on the simulated data.

TABLE IV
TEST RESULTS OF SIMULATION DATA

Simulation data	$Acc/\%$	$Pre/\%$	$Sens/\%$	$F_1/\%$	$Spec/\%$
Simulation data from the training set	100	100	100	100	100
Simulation data from the test set	100	100	100	100	100

$$\begin{aligned}
 Acc &= \frac{TP + TN}{TP + TN + FP + FN} \times 100\% \\
 Pre &= \frac{TP}{TP + FP} \times 100\% \\
 Rec &= Sens = \frac{TP}{TP + FN} \times 100\% \\
 F_1 &= \frac{2 * Pre * Rec}{Pre + Rec} \times 100\% \\
 Spec &= \frac{TN}{TN + FP} \times 100\%
 \end{aligned} \tag{6}$$

B. Full-scale test

The network structure employed in the full-scale test is depicted in Fig. 7, with a total of four feeders. The grounding medium includes grass and sand, tree branches, brick and stone, and so on, as shown in Fig. 8.

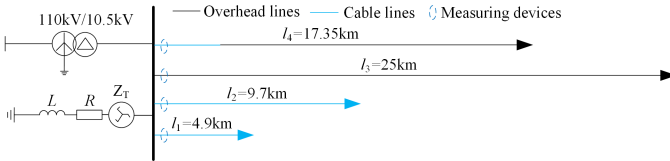


Fig. 7. Network structure of full-scale test

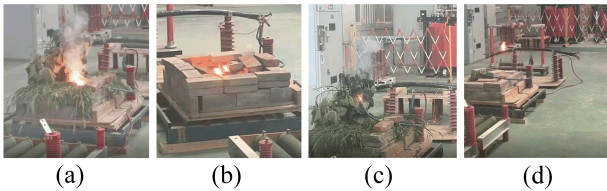


Fig. 8. Full-scale test

(a) Grounding via grass and sand (b) Grounding via brick and stone (c) Grounding via tree branches (d) Grounding via cable arc

The ZSV and ZSC data for the half and one cycle after the fault point were selected and processed in different data processing methods, using the same training strategy and the same computational environment to train the models separately. Afterward, the full-scale test data was used for testing on a Raspberry Pi 4B. The number of test samples is 480, with a ratio of 1:3 between faulty feeder and sound feeder samples. The outcomes of the tests are presented in Table V. Each row in Table V presents the test results of full-scale test data under different data processing methods. The duo/dt indicates whether the ZSV has been subjected to derivative operation, where "Yes" signifies differentiation has been performed, and "No" indicates otherwise. The L indicates the selected data length, which includes a half-cycle after the fault point and one-cycle after the fault point. The F indicates the filtering cut-off frequency, where "-" signifies no filtering.

TABLE V

TEST RESULTS OF FULL-SCALE TEST DATA UNDER DIFFERENT
DATA PROCESSING METHODS

duo/dt	L/cycle	F/Hz	$Acc/\%$	$Pre/\%$	$Sens/\%$	$F_1/\%$	$Spec/\%$
Yes	1	-	99.167	100	96.667	98.305	100
Yes	0.5	-	96.458	99.048	86.667	92.444	99.722
Yes	1	2k	99.375	100	97.5	98.734	100
Yes	0.5	2k	96.875	99.065	88.333	93.392	99.722
Yes	1	75	98.958	98.319	97.5	97.907	99.444
No	1	-	94.375	98.947	78.333	87.442	99.722

From the results of Table V, the algorithm is significantly more effective after performing the derivative operation on the ZSV. The selection of data length is also important. The algorithm's performance is noticeably better when transient waveforms of one-cycle after the fault point are chosen compared to transient waveforms of half-cycle after the fault point. This is because the ZSC undergoes an oscillatory process during a metallic ground fault, while during a high impedance fault, the transient process is longer. Therefore, a notable distinction can be observed in the superimposed waveform of the transient half-cycle and one-cycle ZSV derivatives and ZSC for the faulty feeder and sound feeders. It is feasible to extract data for half-cycle and one-cycle after the fault point. However, since the proposed method classifies based on the number of pixels occupied by different categories, a larger data range provides more fault tolerance when some waveforms are misclassified due to waveform distortion and start-up moment errors. Therefore, extracting data for one cycle after the fault point can yield better results. The filtering processing has less impact on the algorithm's effectiveness. Since filtering out harmonics above 2 kHz, taking the derivative of the ZSV, and taking data from one cycle after the fault point as input to the FCN gave better results, subsequent data processing was carried out using this method.

The model utilized in this paper was trained on simulated data and subsequently tested using full-scale test data. If the model is trained using full-scale test data, when tested again on full-scale test data, metrics such as accuracy, sensitivity, specificity, etc., for feeder detection can reach 100%.

C. Adaptability of feeder detection method

Consider the possible influencing factors of the feeder detection method in engineering applications. Modify the network structure of the distribution network model in Fig. 6, changing the number of feeders from 6 to 10, simulate and obtain simulation data to validate the adaptability of the feeder detection method. The number of simulation data used for testing is 1026, which includes low resistance ground fault and high impedance fault. The proposed method is tested for its ability to correctly identify faulty feeder in the presence of noise interference, sampling asynchrony, etc.

1) Environmental noise

In engineering applications, external noise may introduce interference to the signal, thereby affecting the accuracy of feeder detection. To assess the impact of noise on the proposed method in this paper, Gaussian white noise with signal-to-noise ratios of 20 dB, 30 dB, 40 dB, and 60 dB was respectively introduced into the simulated data for testing. The testing results are presented in Table VI. With the introduction of noise ranging from 30dB to 60dB, there was no change in the accuracy of feeder detection. Only when 20dB of noise was added did the accuracy experience a slight decrease, indicating that noise has minimal impact on the method proposed in this paper.

TABLE VI
TEST RESULTS OF SIMULATION DATA UNDER NOISE
INTERFERENCE

Noise/dB	Acc/%	Pre/%	Sens/%	F ₁ /%	Spec/%
20	99.903	100	99.735	99.868	100
30	100	100	100	100	100
40	100	100	100	100	100
60	100	100	100	100	100

2) Sampling asynchrony

In order to assess the impact of asynchronous sampling on the proposed method in this paper, the sampling times for ZSV and ZSC offsets were set at 0.2ms, 0.6ms, and 1ms, respectively. The testing results are presented in Table VII. From the results in Table VII, it can be observed that as the offset time increases, the accuracy of feeder detection decreases. This is because as the time offset increases, the phase relationship between ZSV and ZSC differs more from the original unshifted state, and the characteristics displayed in the superimposed waveform image may have become distorted. This makes it difficult for the algorithm to correctly identify the faulty feeder.

TABLE VII
TEST RESULTS OF SIMULATION DATA IN THE CASE OF
ASYNCHRONOUS SAMPLING

Offset type	Offset time/ms	Acc/%	Pre/%	Sens/%	F ₁ /%	Spec/%
Current lag voltage	0.2	99.903	100	99.735	99.868	100
	0.6	97.758	95.165	98.942	97.017	97.068
	1	96.979	95.538	96.296	95.916	97.377
Voltage lag current	0.2	100	100	100	100	100
	0.6	98.733	100	96.561	98.25	100
	1	97.368	96.8	96.032	96.414	98.148

3) Inaccurate start-up moment

Currently, the majority of feeder detection methods rely on transient characteristics, and the deviation between the start-up moment and the actual fault moment has a significant impact on transient-based methods. In order to test the performance of the proposed method in this paper under an inaccurate start-up moment, deviations between the start-up moment and the actual fault moment were set at 1ms, 3ms, and 5ms, respectively. The test results are shown in Table VIII. When the actual fault moment lags behind the start-up moment, the captured waveform includes a portion before the actual fault moment and a portion after it. Due to the pronounced transient features in the captured waveform, the accuracy of feeder detection can reach 100%. When the start-up moment lags behind the actual fault moment, there is a slight decrease in accuracy. The misclassified samples share a common characteristic: they all have very low transition impedance. This is because when the transition impedance is low, the transient process of a SPGF is relatively short. If the start-up moment lags significantly behind the actual fault moment, the captured waveform may be closer to a steady-state waveform. This can lead the method proposed in this paper to erroneously classify the faulty feeder as a sound one. When the transition impedance is relatively high, the transient process of a SPGF is longer. Even if the start-up moment lags behind the actual fault moment, the captured waveform still exhibits prominent transient features. In such cases, the method proposed in this paper can still accurately identify the faulty feeder.

TABLE VIII
TEST RESULTS OF SIMULATION DATA IN THE CASE OF
INACCURATE START-UP MOMENT

Deviation type	Deviation time/ms	Acc/%	Pre/%	Sens/%	F ₁ /%	Spec/%
start-up moment	1	99.513	100	98.677	99.334	100
lag the actual	3	97.661	100	93.651	96.721	100
moment of failure	5	95.906	100	88.889	94.118	100
the actual moment	1	100	100	100	100	100
of failure lag	3	100	100	100	100	100
start-up moment	5	100	100	100	100	100

4) Different sampling frequency

In practical applications, there are differences in the sampling frequencies of various data acquisition devices. To assess the impact of sampling frequency on the method proposed in this paper, simulations were conducted at sampling frequencies of 2kHz, 4kHz, 5kHz, and 10kHz. Simulated data was collected and subjected to testing. The test results are shown in Table IX. At sampling frequencies of 4 kHz, 5 kHz, and 10 kHz, the accuracy of feeder detection is 100%. This is because the method proposed in this paper involves the conversion of waveform data into images, thereby reducing the demands on sampling frequency. However, this does not completely eliminate the influence of sampling frequency. At 2kHz, there is a slight decrease in the accuracy of feeder detection. This could be attributed to the low sampling frequency, which result in the loss of some details in the superimposed waveform image, consequently reducing the accuracy of feeder detection.

TABLE IX
TEST RESULTS OF SIMULATION DATA WITH DIFFERENT
SAMPLING FREQUENCY

Sampling frequency/kHz	Acc/%	Pre/%	Sens/%	F ₁ /%	Spec/%
2	99.61	99.471	99.471	99.471	99.691
4	100	100	100	100	100
5	100	100	100	100	100
10	100	100	100	100	100

D. Comparison of methods

Full-scale test data was used to test the proposed method in this paper, and a comparison was conducted against methods [8], [18], [19], and [20]. The outcomes are presented in Table X.

TABLE X
COMPARATIVE ANALYSIS OF FEEDER DETECTION METHODS

method	Acc/%	Pre/%	Sens/%	F ₁ /%	Spec/%
Guo et al. [8]	87.083	82.222	61.667	70.476	95.556
Feng et al. [18]	94.167	100	76.667	86.792	100
Wei et al. [19]	84.583	69.167	69.167	69.167	89.722
Yuan et al. [20]	83.333	67.857	63.333	65.517	90
Proposed method	99.375	100	97.5	98.734	100

Guo et al. [8] converted ZSC into a time-frequency grayscale image and then utilized CNN for feeder detection. This method transformed ZSC into time-frequency grayscale images, providing a more intuitive display of features. However, the time-frequency transformation may result in some loss of useful features[21]. Feng et al. [18] performed a least-squares linear fit to the transient ZSV derivative, the ZSC, and the feeder detection results depend on the fit function's slope. This method employed a single feature for

feeder detection. While the approach is simple, the universality of this feature contributes to its effectiveness in feeder detection. Feng et al. [18] misclassified some faulty feeders as sound feeders, and some waveforms are depicted in Fig. 9. From the waveform point of view, this is mainly due to distortion of the faulty feeder ZSC waveform and the effect of start-up moment errors. Wei et al. [19] employed the multiple evidence estimation method to fuse transient energy, kurtosis value, and cross-correlation distance, selecting the feeder with the maximum fault degree as the faulty feeder. This method fused three transient features, which may lead to more reliable results in feeder detection compared to methods relying on individual features. Yuan et al. [20] utilized variational mode decomposition to acquire the cross-correlation coefficients of feeders, and subsequently employed these coefficients along with harmonic energy for faulty feeder detection. This method is applicable to distribution networks with distributed power sources.

The method proposed in this paper leverages the relationship between transient ZSV derivatives and transient ZSC for feeder detection, a relationship characterized by broad applicability. Compared to the manually extracted individual features in Feng et al. [18], the algorithm used in this paper extracts more comprehensive features, leading to enhanced accuracy in feeder detection. Furthermore, the proposed method exhibits strong resistance to interference, enabling accurate identification of faulty feeder even in scenarios involving noise interference and inaccurate start-up moment, etc.

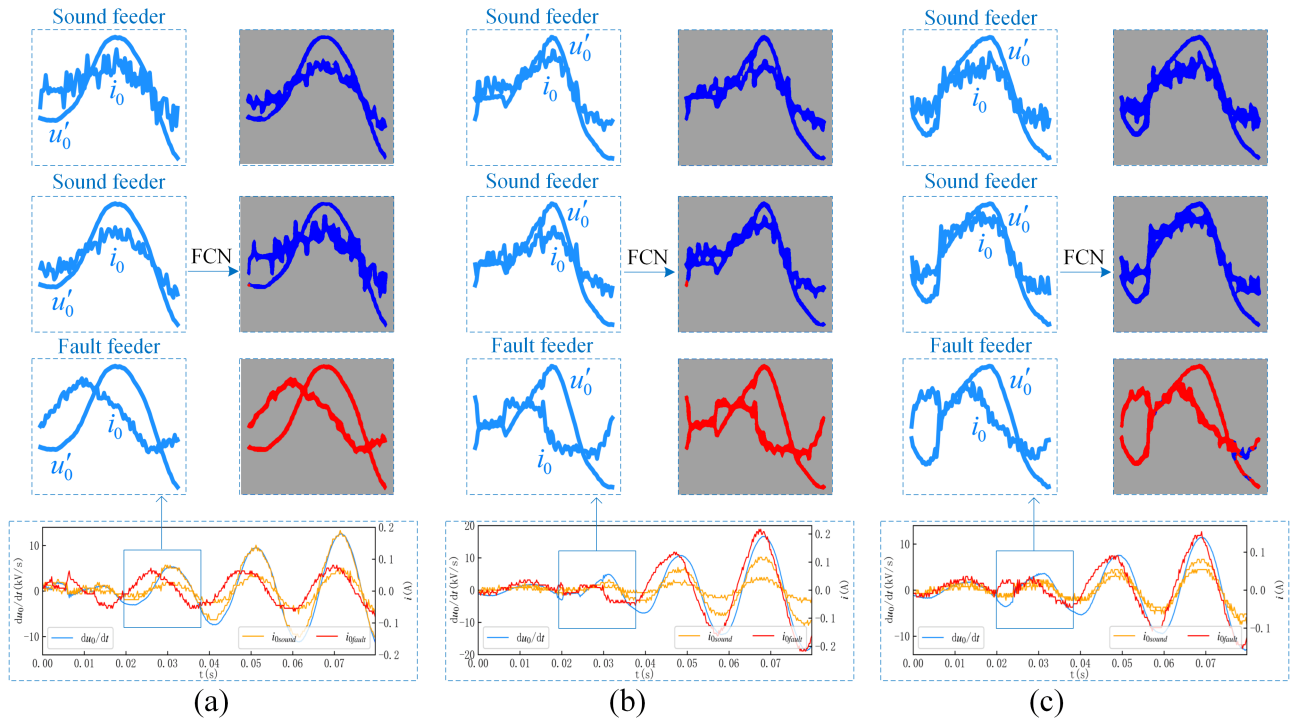


Fig. 9. Waveform superimposition image and corresponding segmentation results.
(a) Grounding via tree branches (b) Grounding via grassy sandy sand (c) Grounding via tree branches

V. CONCLUSION

This paper utilizes FCN to implement SPGF feeder detection. FCN is used to classify each pixel in the input image. Detecting faulty feeder based on the number of pixels of different categories in the segmentation map output by FCN can make the final decision of feeder detection more transparent and easily understandable. Furthermore, the proposed method doesn't entail setting thresholds, thus avoiding the influence of threshold selection on the results of feeder detection.

Tests were conducted to validate the performance of the proposed method, using both simulated and field data. The outcomes demonstrate the proposed method is able to adapt to scenarios such as noise interference, sampling asynchrony, etc., and has strong anti-interference and generalization capabilities. The proposed method remains capable of accurately identifying faulty feeder, even in cases where there is a deviation between the start-up moment and the actual fault moment.

REFERENCES

- [1] L. He et al., "Single-Phase to Ground Fault Line Identification for Medium Voltage Islanded Microgrids With Neutral Ineffectively Grounded Modes," *IEEE Trans. Smart Grid*, vol. 13, no. 6, pp. 4312-4326, 2022, doi: 10.1109/TSG.2022.3176000.
- [2] X. Zeng, K. Yu, Y. Wang, and Y. Xu, "A novel single phase grounding fault protection scheme without threshold setting for neutral ineffectively earthed power systems," *CSEE J. Power Energy Syst.*, vol. 2, no. 3, pp. 73-81, 2016, doi: 10.17775/CSEEJPES.2016.00038.
- [3] P. Liu and C. Huang, "Detecting Single-Phase-to-Ground Fault Event and Identifying Faulty Feeder in Neutral Ineffectively Grounded Distribution System," *IEEE Trans. Power Deliv.*, vol. 33, no. 5, pp. 2265-2273, 2018, doi: 10.1109/TPWRD.2017.2788047.
- [4] X. Wang et al., "Location of Single Phase to Ground Faults in Distribution Networks Based on Synchronous Transients Energy Analysis," *IEEE Trans. Smart Grid*, vol. 11, no. 1, pp. 774-785, 2020, doi: 10.1109/TSG.2019.2938667.
- [5] X. Wei et al., "Faulty Feeder Detection for Single-Phase-to-Ground Fault in Distribution Networks Based on Transient Energy and Cosine Similarity," *IEEE Trans. Power Deliv.*, vol. 37, no. 5, pp. 3968-3979, 2022, doi: 10.1109/TPWRD.2022.3142186.
- [6] N. Peng et al., "Single-Phase-to-Earth Faulty Feeder Detection in Power Distribution Network Based on Amplitude Ratio of Zero-Mode Transients," *IEEE Access*, vol. 7, pp. 117678-117691, 2019, doi: 10.1109/ACCESS.2019.2936420.
- [7] H. Okumus and F. M. Nuroglu, "A random forest-based approach for fault location detection in distribution systems," *Electr. Eng.*, vol. 103, no. 1, pp. 257-264, 2021, doi: 10.1007/s00202-020-01074-8.
- [8] M. Guo, X. Zeng, D. Chen, and N. Yang, "Deep-Learning-Based Earth Fault Detection Using Continuous Wavelet Transform and Convolutional Neural Network in Resonant Grounding Distribution Systems," *IEEE Sens. J.*, vol. 18, no. 3, pp. 1291-1300, 2018, doi: 10.1109/JSEN.2017.2776238.
- [9] J. Yuan and Z. Jiao, "Faulty feeder detection based on image recognition of current waveform superposition in distribution networks," *Appl. Soft. Comput.*, vol. 130, p. 109663, 2022, doi: 10.1016/j.asoc.2022.109663.
- [10] J. Yuan, T. Wu, Y. Hu, and Z. Jiao, "Faulty feeder detection based on image recognition of voltage-current waveforms in non-effectively grounded distribution networks," *Int. J. Electr. Power Energy Syst.*, vol. 143, p. 108434, 2022, doi: 10.1016/j.ijepes.2022.108434.
- [11] J. Yuan and Z. Jiao, "Faulty feeder detection for single phase-to-ground faults in distribution networks based on patch-to-patch CNN and feeder-to-feeder LSTM," *Int. J. Electr. Power Energy Syst.*, vol. 147, p. 108909, 2023, doi: 10.1016/j.ijepes.2022.108909.
- [12] J. Gao, M. Guo, and D. Chen, "Fault line detection using waveform fusion and one-dimensional convolutional neural network in resonant grounding distribution systems," *CSEE J. Power Energy Syst.*, vol. 7, no. 2, pp. 250-260, 2020, doi: 10.17775/CSEEJPES.2020.02560.
- [13] J. Yuan and Z. Jiao, "Faulty feeder detection based on fully convolutional network and fault trust degree estimation in distribution networks," *Int. J. Electr. Power Energy Syst.*, vol. 141, p. 108264, 2022, doi: 10.1016/j.ijepes.2022.108264.
- [14] L. Chen et al., "EFCNet: Ensemble Full Convolutional Network for Semantic Segmentation of High-Resolution Remote Sensing Images," *IEEE Geosci. Remote Sens. Lett.*, vol. 19, pp. 1-5, 2022, doi: 10.1109/LGRS.2021.3076093.
- [15] Y. Bao, S. Soltanian-Zadeh, S. Farsiu, and Y. Gong, "Segmentation of neurons from fluorescence calcium recordings beyond real time," *Nat. Mach. Intell.*, vol. 3, no. 7, pp. 590-600, 2021, doi: 10.1038/s42256-021-00342-x.
- [16] C. Lin, W. Gao, and M. Guo, "Discrete Wavelet Transform-Based Triggering Method for Single-Phase Earth Fault in Power Distribution Systems," *IEEE Trans. Power Deliv.*, vol. 34, no. 5, pp. 2058-2068, 2019, doi: 10.1109/TPWRD.2019.2913728.
- [17] Q. Zhang, Q. Yuan, J. Li, Z. Yang, and X. Ma, "Learning a Dilated Residual Network for SAR Image Despeckling," *Remote Sens.*, vol. 10, no. 2, p. 196, 2018, doi: 10.3390/rs10020196.
- [18] G. Feng et al., "Grounding Fault Line Selection of Non-solidly Grounding System Based on Linearity of Current and Voltage Derivative," *Power System Technology*, vol. 45, no. 1, pp. 302-311, 2021, doi: 10.13335/j.1000-3673.pst.2019.1272.
- [19] X. Wei et al., "Faulty Feeder Detection Based on Fundamental Component Shift and Multiple-Transient-Feature Fusion in Distribution Networks," *IEEE Trans. Smart Grid*, vol. 12, no. 2, pp. 1699-1711, 2021, doi: 10.1109/TSG.2020.3026390.
- [20] J. Yuan, Y. Hu, Y. Liang, and Z. Jiao, "Faulty Feeder Detection for Single Line-to-Ground Fault in Distribution Networks With DGs Based on Correlation Analysis and Harmonics Energy," *IEEE Trans. Power Deliv.*, vol. 38, no. 2, pp. 1020-1029, 2023, doi: 10.1109/TPWRD.2022.3203992.
- [21] S. Huang, J. Tang, J. Dai, and Y. Wang, "Signal Status Recognition Based on 1DCNN and Its Feature Extraction Mechanism Analysis," *Sensors*, vol. 19, no. 9, p. 2018, 2019, doi: 10.3390/s19092018.



Cui Hong was born in Xining, Qinghai, China in 1972. She received the B.S degree in Power System Automation from the Fuzhou University, China, in 1994, and she received M.S. and Ph.D degrees in Electrical Machinery and Electrical Appliances from Fuzhou University too, in 2000 and 2014 respectively. Currently, she is an associate professor in School of Electrical Engineering and Automation at Fuzhou University. Her main research interest includes fault diagnosis of distribution network and its main equipment, new energy power and load forecasting and so on.



Heng-Yi Qiu was born in 1998 in Fujian Province, China. He received his Bachelor's degree in Electrical Engineering from Fuzhou University, China in 2021. He is currently pursuing a Master's degree in Electrical Engineering at Fuzhou University. His research interests include power distribution systems and their automation, and the application of artificial intelligence in power distribution systems.



Jian-Hong Gao was born in Fuzhou, China, in 1994. He received the B.S. in electrical engineering from Shanghai University of Electric Power, Shanghai, China, in 2017. He is currently pursuing the Ph.D. degree in electrical engineering with Fuzhou University and the Ph.D. degree in electrical engineering with Yuan

Ze University. His research interests include power distribution systems and its automation, application of artificial intelligence in power distribution systems.



Shuyue Lin is a lecturer in electrical and electronic engineering at the University of Hull, UK. Before that, she was an assistant professor at Fuzhou University, China. She obtained her PhD in engineering (University of Warwick), MSc in control systems (Imperial College London), and BEng in electrical power

engineering (the University of Bath and North China Electric Power University) in 2019, 2013, and 2012, respectively. Her current research interests include power generation and grid integration of renewable energies, fault detection and diagnosis in power systems.



Mou-Fa Guo (Member, IEEE) was born in Fujian province, China, in 1973. He received the B.S. and M.S. degrees in electrical engineering from Fuzhou University, Fuzhou, China, in 1996 and 1999, respectively, and the Ph.D. degree in electrical engineering from Yuan Ze University, Taoyuan, Taiwan, in 2018.

Since 2000, he has been with Fuzhou University, where he is currently a Professor with the College of Electrical Engineering and Automation. His research interests include the information processing, protection control and flexible arc suppression of single -line -to -ground fault in distribution networks.